


Fluorescence Hot Paper

 How to cite: *Angew. Chem. Int. Ed.* **2021**, *60*, 23705–23712

International Edition: doi.org/10.1002/anie.202107436

German Edition: doi.org/10.1002/ange.202107436

Second-Sphere Interaction Promoted Turn-On Fluorescence for Selective Sensing of Organic Amines in a Tb^{III}-based Macrocyclic Framework

Junyu Ren, Zheng Niu, Yingxiang Ye, Chen-Yen Tsai, Shixi Liu, Qingzhi Liu, Xianqiang Huang, Ayman Nafady, and Shengqian Ma*

Abstract: Guided by a second-sphere interaction strategy, we fabricated a Tb(III)-based metal–organic framework (MMCF-4) for turn-on sensing of methyl amine with ultra-low detection limit and high turn-on efficiency. MMCF-4 features lanthanide nodes shielded in a nonacoordinate geometry along with secondary coordination spheres that are densely populated with H-bond interacting sites. Nonradiative routes were inhibited by binding-induced rigidification of the ligand on the second coordination sphere, resulting in luminescence amplification. Such remote interacting mechanism involved in the turn-on sensing event was confirmed by single-crystal X-ray diffraction and molecular dynamic simulation studies. The design of both primary and secondary coordination spheres of Tb(III) enabled the first turn-on sensing of organic amines in aqueous conditions. Our work suggests a promising strategy for high-performance turn-on sensing for Ln-MOFs and luminous materials driven by other metal chromophores.

Introduction

Molecular recognition has attracted much attention in various fields including chemo-sensing ever since its initial designation to understand biological process.^[1] Compared with other chemo-sensors, luminescence materials have been greatly envisioned owing to their advantages of easy handling, quick response, and high sensitivity. To date, most reported mechanisms in this field involve a turn-off optical signal, where the fluorescence is quenched by the analytes via photoinduced electron or energy transfer, thus limiting their practical applications.^[2] Although the sensing process of a fluorescence sensor is defined by the chemistry of the

binding site and signaling center, they are also markedly influenced by the way the two components communicate as well as the local environment that they experience.^[3] Therefore, the ability to layout novel corresponding mode and assembly pattern between the two constituents would be an appealing proposition with perspective of the realization of turn-on sensing phenomenon with higher fidelity.^[4] Nonetheless, easy access to novel chemo-sensors in traditional chemo-sensory systems was hindered due to the requirement of complicated chemical modification of components, and thereby prompting the need for innovative technologies.

Metal–organic frameworks (MOFs), as one category of custom-designed porous materials, possessing tunable pore size and various designable binding sites, offer a great opportunity to introduce molecular recognition and to develop functional sensing materials.^[8] Benefiting from the unique metal centered emission, lanthanide metal-organic frameworks (Ln-MOFs) have long been widely investigated for the detection of anions, temperature, pH variation, explosives, cancer biomarkers and toxic contaminants.^[9] However, compared with other sensing mechanisms in Ln-MOFs, it is much easier to trigger the cut-off of the antenna effect by photoinduced electron transfer (PET) and fluorescence resonance energy transfer (FRET), which leads to Ln-sensors with a quenching behavior.^[5] Therefore, sensing with enhancement of fluorescence-intensity in Ln-MOFs remains a challenge, and is much more scarce compared with MOFs featuring ligand-centered luminescence (Table 1).^[5–7,10] Practically, luminescence enhancement in Ln-sensors can be possible when i) analytes function as an antenna, or ii) chromophore being effectively modulated via host-guest interactions.^[11] However, the deactivating effect from prox-

[*] J. Ren, Dr. Y. Ye, Prof. S. Ma
 Department of Chemistry, University of North Texas
 Denton, TX 76203-5070 (USA)
 E-mail: Shengqian.Ma@unt.edu

Prof. Z. Niu
 College of Chemistry, Chemical Engineering and Materials Science
 Soochow University, Suzhou 215123 (China)

Prof. X. Huang
 Shandong Provincial Key Laboratory of Chemical Energy Storage and
 Novel Cell Technology, School of Chemistry & Chemical Engineering
 Liaocheng University, Liaocheng 252059 (China)

Prof. Q. Liu
 College of Chemistry and Pharmaceutical Science
 Qingdao Agriculture University
 No. 700 Changcheng Road, Qingdao City 266109 (China)

Prof. C. Tsai
 Department of Chemistry, Chinese Culture University
 Taipei (Taiwan)

Prof. S. Liu
 School of Chemical Science and Technology, Yunnan University
 2 North Road of Green Lake, Kunming 650091, Yunnan (China)

Prof. A. Nafady
 Department of Chemistry, College of Science, King Saud University
 Riyadh 11451 (Saudi Arabia)



 Supporting information and the ORCID identification number(s) for the author(s) of this article can be found under:
 <https://doi.org/10.1002/anie.202107436>.

Table 1: Ln-MOFs with turn-on sensing behaviors toward organic molecules.

Compound	Analyte	Mechanism	Coordinated guest molecule	Sensing environment	Ref.
[Eu ₂ (L') ₃ (H ₂ O) ₄] ₃ ·3 DMF	DMF vapor	media effect	H ₂ O	air	[5]
Eu(NH ₂ BTC)(H ₂ O)·(H ₂ O)(DMF) ₂	dipicolinic acid	antenna effect	H ₂ O	ethanol	[6]
Yb-NH ₂ -TPDC	gossypol	antenna effect	H ₂ O or DMF	acetone	[7]
[Tb ₂ (L) ₂](H ₂ O) _n	methylamine	second-sphere interactions	none	H ₂ O	This work

*L' denotes 2',5'-bis(methoxymethyl)-[1,1':4',1''-terphenyl]-4,4''-dicarboxylate, L denotes 5,5',5''-(1,4,7-triazonane-1,4,7-triyl)tris(methylene)trisophthalate.

imate XH oscillators (X=O or N, especially OH in H₂O), which is an intrinsic deficiency for most Ln-sensors, largely minimizes the scope of applications for Ln-MOFs.^[12] To avoid the deactivating effect from quenchers, the performing Ln-MOFs would prefer an inaccessible lanthanide node which nonetheless exhibits effective correspondence with binding sites outside first-coordination sphere.

It is generally known from lanthanide chemistry that the emission center needs effective shielding in aqueous environment to avoid deactivating effect from proximate OH oscillators. This requires a saturated first coordination sphere, suggesting Ln³⁺ exist in an eight or even nine coordination geometry.^[12a] Under the premise of inaccessible first coordination sphere, we consider decorating the secondary coordination sphere with proper functional sites thus to carry out recognition event via second-sphere interactions^[13] (Figure 2a). The most commonly studied ligands for lanthanide luminescence are polyamine derivatives, which commonly host Ln³⁺ in its cavity to form high coordination lanthanide complexes.^[12] In rare cases, Ln³⁺ could only coordinate with the side-arms while aza-macrocycles merely serve as part of antenna and do not directly interact with metal ion.^[14] Side-chain carboxylic acid can bind Ln³⁺ either in monodentate or bidentate coordination mode. Each of the monodentate coordination generates a dangling oxygen site in situ, serving as potential H-bond interaction sites in second coordination sphere, which can satisfy the very demand of our strategy. For bidentate coordination, it could complete coordination sphere efficiently to afford a saturated inner-sphere.^[15]

Organic amines are well-known for their toxicity to human health and harmfulness to the environment. As one of the most applied amines in industry, methyl amine (MA) is associated with a variety of environmental pollution, food contamination and cancer biomarkers.^[16] Even so, selective fluorescent sensing of methyl amine, especially with a turn-on behavior, remains undeveloped.^[8i] Additionally, the NH oscillators in amine is itself an oscillating quencher toward lanthanide emission, and thus the turn-on sensing of methyl amine would be more challenging and attractive. Therefore, as a better evidence for the concept of our strategy, we selected methyl amine (MA) as the analyte in this endeavor.

Bearing those above considerations in mind, we designed and synthesized a Tb(III)-based macrocyclic frameworks MMCF-4 (MMCF denotes metal-macrocyclic framework) comprising the desired nona-coordinate terbium node, as well as a secondary coordination sphere densely populated with H-bond interacting sites (Ligand H₆L is shown in Figure 1a, Tb³⁺ node and H-bond receptor are shown in Figure 1b), aiming for turn-on sensing and antijamming property in Ln-MOFs. The proposed material MMCF-4 achieves turn-on sensing toward methyl amine (MA) in aqueous solution, with an ultra-low detection limit of 86 nM. The strong H-bond interactions between MA molecules and MMCF-4 induce rigidification of the soft ligand, thus boosting sensitization of the emission center and lead to a significant enhancement of luminescence. This was clearly confirmed by single crystal X-ray diffraction (SCXRD) studies and molecular dynamic simulations. Moreover, this second-sphere interaction can be

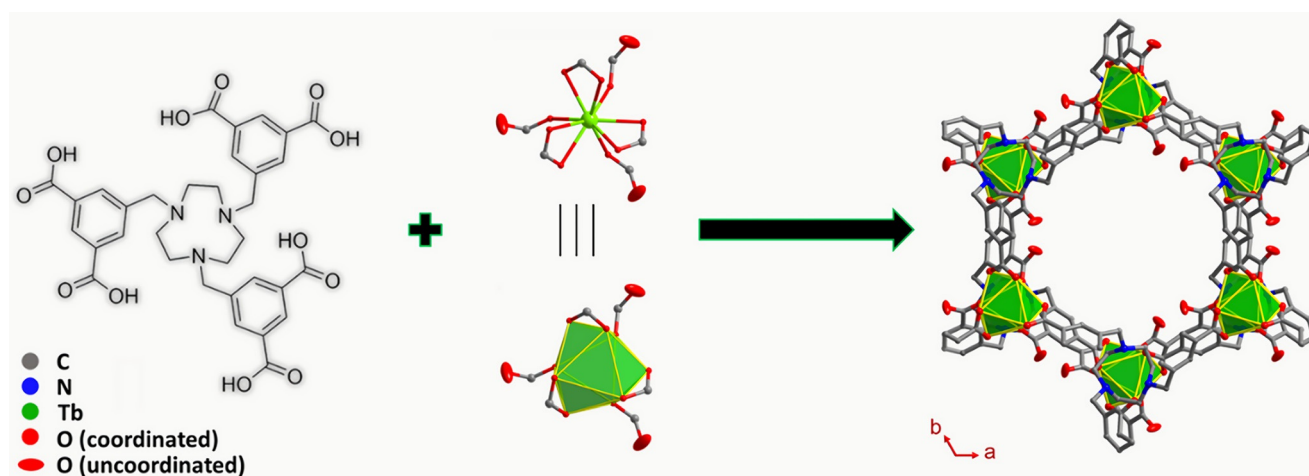


Figure 1. Representation of the assembly of MMCF-4 and structure details. Structures of a) H₆L; b) 9-coordinated terbium node; c) MMCF-4 structures viewed along the c-axis.^[22]

transferable to a turn-off sensing of 6-mercaptopurine, a widely applied chemotherapeutic agent, with a detection limit of 44.6 nM. This initial work opens a new gate for the application of lanthanide-chromophores in highly sensitive detection of organic analytes with enhanced fluorescence intensity.

Results and Discussion

Solvothermal reaction of H_6L with $Tb(NO_3)_3 \cdot 6H_2O$ in DMF solution at 120 °C for 1 week afforded colorless needle-shaped crystals of MMCF-4 (Figure S1). SCXRD revealed MMCF-4, with the formula of $[Tb(L)] \cdot (H_2O)_n$ ($H_6L = 5,5',5''$ -((1,4,7-triazonane-1,4,7-riyl)tris(methylene))trisisophthalic acid) crystallizes in the hexagonal space group of $P31c$. It is worth noting that Tb^{3+} does not go inside the ligand cavity, but resides ca. 6.5 Å away from the aza-macrocyclic through coordination only with carboxyl groups. Compared with the high coordination pattern achieved by a single ligand, this actually provides necessary metal sites to extend to a 3D framework. In the structure, the Tb^{3+} ions show a 9-coordinated, tricapped trigonal prismatic geometry, where each Tb^{3+} ion connects with six carboxyl groups, of which three coordinate in monodentate mode and the other three chelate in bidentate mode (Figure S4). The Tb^{3+} ion is bridged by the isophthalic acid moieties of the L in an asymmetric fashion (one end in monodentate mode, the other in bidentate mode) to form infinite one-dimensional channels, with an aperture of ca. 15 Å, along c direction (Figure 1c). From the topological viewpoint, if L and Tb are simplified as 4- c nodes, the framework would be a uninodal (4,4)- c net (lon-type) with point symbol of $\{6^6\}$ (Figure S3). The total solvent-accessible volume in MMCF-4 framework is estimated to be 48.6%.

Thermogravimetric analysis (TGA) showed that MMCF-4 could be stable up to ca. 200 °C (Figure S5). The phase purity of the prepared bulk products was verified by a comparison of the experimental and calculated powder X-ray diffraction (PXRD) patterns (Figures S8). Albeit MMCF-4 is built from the flexible ligand H_6L , it still demonstrates excellent chemical stability in various solvents and aqueous solutions of a wide pH range (pH 3–12) (Figure S11, S12). This could be attributed to high coordination metal node which can sustain itself in harsh environments and form a stable framework since most collapses start from attacks on the metal node.^[17] PXRD results confirmed that the structure of MMCF-4 is maintained after exposure to the above conditions as well as air/water for at least one year. To assess its permanent porosity, the titled sample was guest-exchanged with CH_3OH and then activated by supercritical CO_2 method to yield the guest-free phase. N_2 adsorption isotherms of the guest-free material were measured at 77 K (Figure S9). Based on the N_2 adsorption data, a Brunauer–Emmett–Teller (BET) surface of 612 $m^2 g^{-1}$ was calculated for MMCF-4. Furthermore, the N_2 sorption isotherms for the samples after being soaked in water, boiling water, pH 3 HCl aqueous solution, and pH 12 NaOH aqueous solution for 24 h were measured and almost the same isotherms were observed as that of the pristine sample (Figure S14). These findings verified the

excellent chemical stability of MMCF-4 under those conditions.

The UV/Vis absorption spectra of H_6L and MMCF-4 were collected using a Shimadzu UV-3600 spectrophotometer. H_6L shows an absorption range between 250 nm and 350 nm, with the highest absorption peak located at 285 nm, while the highest absorption of MMCF-4 redshifted to 312 nm. Based on the 2D excitation-emission map of MMCF-4, 270 nm is determined as the optimal excitation wavelength for efficient emission (Figure S16, S23). When excited at 270 nm, MMCF-4 exhibits the characteristic lanthanide luminescence of terbium ion within 450–660 nm in both solid state and aqueous suspensions (Figure 2c). Four well-resolved characteristic emission peaks were observed at 488, 546, 583, and 621 nm, which stem from the $^5D_4 \rightarrow ^7F_J$ ($J = 6, 5, 4, \text{ and } 3$) transitions of Tb^{3+} , with the emission maximum located at 546 nm.

It is reasonable to anticipate that the densely populated H-bond interacting sites within MMCF-4 will strongly favor noncovalent interactions between the analyte and the ligand to form second-sphere adducts. As a flexible ligand, H_6L would show certain levels of intramolecular freedom when participating in the construction of the framework. Within MMCF-4, the monodentate coordinating mode further increases the linker freedom and enables different activating efficiency of L as antenna before and after constraint of its configuration. Accordingly, MMCF-4 possesses potential as turn-on luminescence sensor when it comes to the restriction of its conformation.

During titrations, fluorescence intensity of MMCF-4 was recorded after addition of each equivalent analyte portion. Continuous enhancement of fluorescence intensity in MMCF-4 aqueous suspension was observed upon the increasing addition of methyl amine (0–60 μM) (Figure 2b,d). A linear response between the fluorescent intensity at 546 nm and the MA concentration fits well with $R^2 = 0.9950$ in the range of 0–30 μM (Figure S20). The detection limit was calculated by the equation $LOD = 3S_b/\text{slope}$, where S_b is the standard deviation of the blank signal and slope was obtained from the linear fit of the concentration-dependent luminescence intensity curve monitored at 546 nm. The detection limit was calculated to be 86 nM for MA (Figure S20). Notably, a saturation of the turn-on titration was observed here, when the mole ratio of MA to L was beyond ca. 3:1. The fluorescence intensity will not vary anymore even with higher analyte concentration. For example, in 2 mL aqueous suspension with ca. 0.035 mg MMCF-4, the saturation concentration for MA is around 60 μM . Since there are three interacting sites on each L, this also suggests the role of pendant carboxylic moieties in the process of turn-on sensing. At the saturation point, the intensity of the 546 nm peak reached to ca. 260% compared with the MMCF-4 suspension without MA.

According to previous studies, the efficiency of vibrational energy transfer from an excited lanthanide ion to proximate OH/NH oscillators decreases greatly with distance.^[12a] To evaluate the effect of lattice water experimentally, guest-free MMCF-4 was obtained and soaked into D_2O to form homogenous suspension. The fluorescence signal was proved

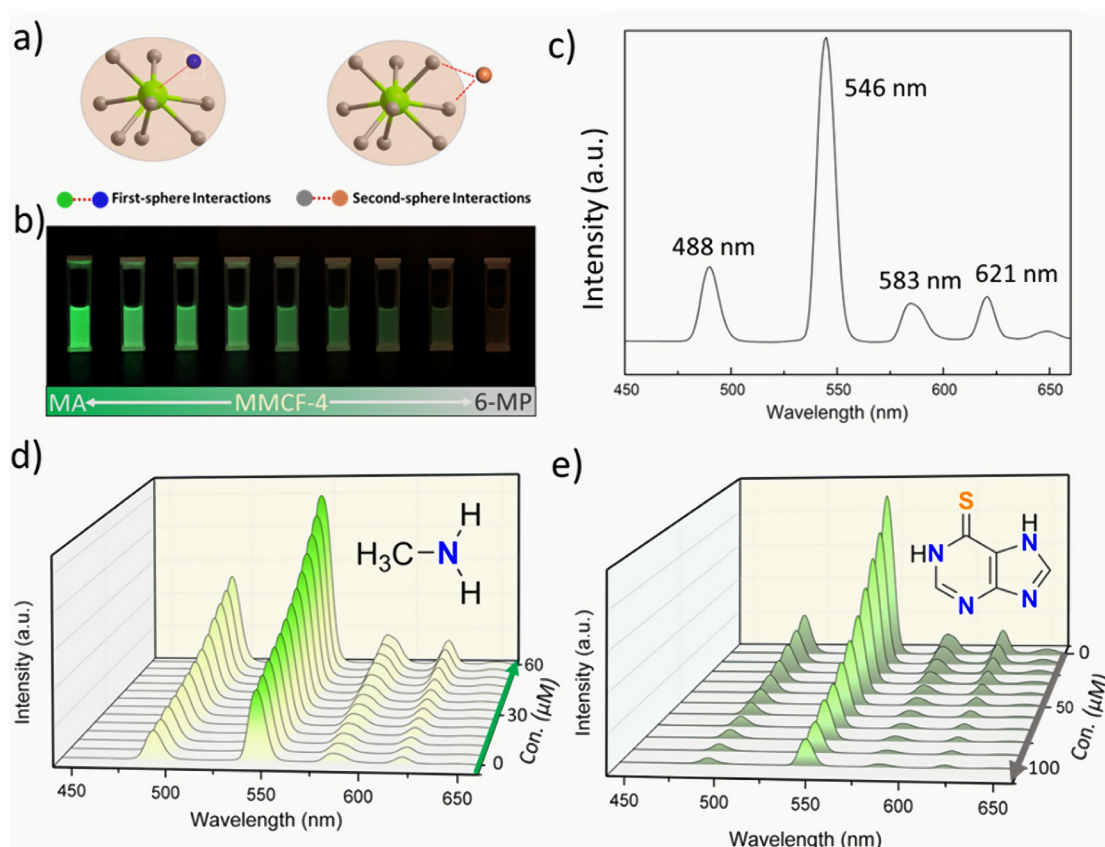


Figure 2. a) Illustration of first/second-sphere interactions. b) Photographs of MMCF-4 in the presence of MA/6-MP with different concentrations under 260 nm UV light. c) Fluorescence spectra of MMCF-4; fluorescence intensity of MMCF-4 aqueous suspension upon addition of d) methylamine and e) 6-mercaptopurine.

to be only slightly influenced by increasing addition of H₂O, as shown in Figure S25, indicating the O-H oscillator deactivation decreases greatly outside the primary coordination sphere. To examine the possible influence of pH in the media caused by the addition of amine, we collected the PL spectra of MMCF-4 in buffer solutions (pH 3 and 12). A negligible variation in fluorescence intensity was noted (Figure S13 in Supporting Information), thereby confirming that a change in pH has little impact on the variations of fluorescence intensity.

To explore the selectivity of MMCF-4 toward analytes, fluorescence experiments were conducted for other organic amines (Figure S28). The results indicated that MMCF-4 is more sensitive toward MA than other tested amines. As common interferences in biological fluids, amino acids were also studied as competing analytes (Figure S29). Since multiple functional groups exist to form complementary interactions, the enhancement of fluorescent intensity could also be observed for amino acids but at much higher concentration of 1 mM with significantly lower turn-on efficiency (i.e. less than 130% intensity enhancement for amino acids vs. 260% intensity enhancement for MA). It is noteworthy that most of them only show turn-on effects with a very low efficiency, and none of them shows a turn-off effect for the emission. Their low turn-on efficiency could be due to the unmatched molecule sizes/geometries, polarities, hydrophilicity/hydro-

phobicity, etc. With the inaccessible primary coordination sphere, Tb emissions will not be disturbed and thus no quenching effect was observed. These results suggest that, to generate sufficient turn-on signal, suitable molecular size and geometries are needed to efficiently interact and suppress the nonradiative pathways inside the channels of MMCF-4.^[8]

With the coordinatively saturated Tb metal nodes in MMCF-4, we also designed experiments for its sensing performance based on photoinduced electron transfer (PET) mechanism. 6-mercaptopurine, as one kind of chemotherapeutic agents, belongs to purine nucleoside analogues and currently is the cornerstone in the treatment protocols of acute lymphocytic leukemia, chronic myeloid leukemia, Crohn's disease, and ulcerative colitis.^[18] In view of its notorious side effects and thus requirement of timely therapeutic drug monitoring (TDM), 6-MP was selected as the analyte.^[19] As shown in Figure 2e, highly efficient luminescent quenching of MMCF-4 was observed upon the addition of 6-MP. The decrease of the maximum fluorescence emission wavelength of 6-MP shows good linearity ($R^2 = 0.9978$) and the detection limit (LOD) was calculated to be 44.6 nM (Figure S21). This result shows the coexistence of two signaling mechanisms in one fluorescence sensor, and also distinguishes MMCF-4 from previous studies, in which the quenching behaviors were ruled not only by PET, but also disturbed by other mechanisms.^[2a]

Based on the MA:L ratio at the saturation point, we deduced that MA could easily diffuse into MMCF-4, due to relatively larger pore-aperture, enabling the interactions between hosted MA molecules and the accessible pendent binding sites within the channels. We speculate H_6L contributes to the turn-on sensing in the following aspects: When serving as the antenna to activate the terbium emission, H_6L is apt to be modulated as sensitizer by virtue of its soft nature. Emission enhancement could be achieved upon binding induced rigidification and suppression of vibration modes responsible for nonradiative decay. Besides, the quenching oscillators (mainly H_2O which interacts with the binding sites) are further blocked away from emission center after the formation of second-sphere adducts between MA and interacting sites, in which the emission will be recovered from resonance energy transfer.

The fluorescence lifetime decays of MMCF-4, MA@MMCF-4 and 6-MP@MMCF-4 in aqueous suspensions were all fitted to monoexponentially curves (Figure S19). The decay of MMCF-4 measured at 270 nm was calculated to be 0.97 ms, and 6-MP@MMCF-4 has a comparable fluorescence lifetime of 0.96 ms. In contrast, the decay of MA@MMCF-4 was determined to be 1.16 ms, much longer than MMCF-4 and 6-MP@MMCF-4, indicating a suppression of non-radiative decay pathways.^[6,10,11]

To elucidate the mechanism under such aliphatic amine-induced luminescence enhancement, evacuated MMCF-4 crystal was soaked in methyl amine solution for direct visualization of the host-guest interactions. MA incorporated MMCF-4 crystals were obtained under identical conditions to fluorescence testing and then applied for single crystal X-ray diffraction studies. The crystal structure clearly shows methyl amine guest molecules held in the hexagonal nanopores of MMCF-4 through N-H...O hydrogen-bonding interactions (Figure 3 a,b). Notably, MA molecules formed bifurcate hydrogen bonds with the accessible oxygen sites from monodentate-coordinating car-

boxylic group and one adjacent oxygen from bidentate-coordinating carboxylic group. The H-bond length between protonated amine and the free/chelate oxygen sites were measured to be 2.63 and 2.74 Å, indicating relatively strong hydrogen bonding interactions (Figure 3b, Table S4).^[20] The ratio of MA molecules toward L in MA@MMCF-4 is 3:1, which correlates well with the results in titration experiments. Besides, no coordinating guest molecule was found in the first coordination sphere of MA@MMCF-4, which further confirms the well-shielding of Tb^{III} center.

To gain insight into the suppression effect of hydrogen bond-formation on the intrinsic vibration modes, molecular dynamic simulations were performed using Forcite module in Materials Studio Package. MMCF-4 and MA@MMCF-4 was described using the universal force field and QEq charges. After optimization, the crystal structures of MMCF-4 and MA@MMCF-4 from SCXRD were applied as the initial structure. The oscillating behaviors within the framework were represented here as the distribution range of torsional degrees (Δt_d), which could be further defined as the degree

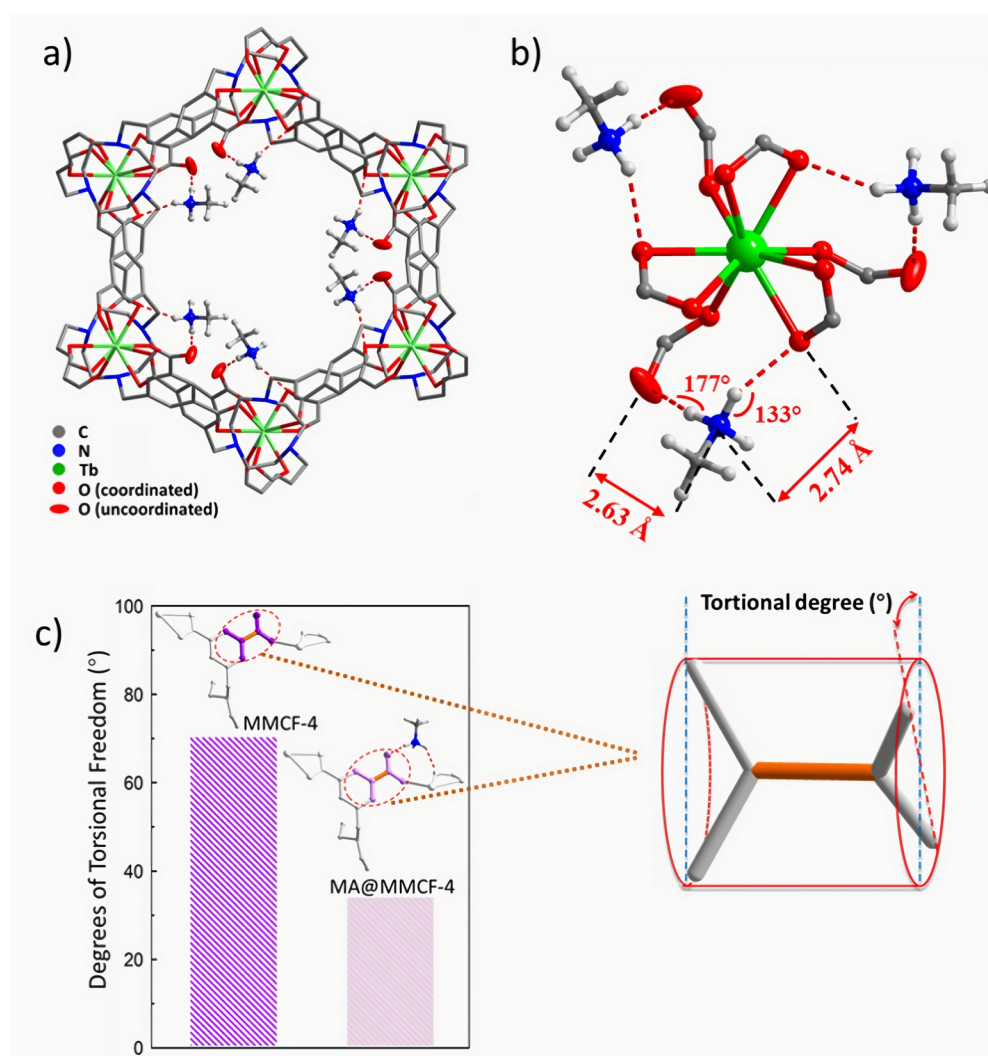


Figure 3. a) Perspective view of a single pore in MA@MMCF-4 adsorbate, along the *c* axis, showing methyl amine guest molecules held in MMCF-4.^[22] b) Details of host-guest interactions in MA@MMCF-4. c) Degrees of torsional freedom for L (illustrated by highlighted bonds) in MMCF-4 and MA@MMCF-4.

range available for torsion between the selected bonds at 298 K (as illustrated in Figure 3c, between color-coded C–O bond on carboxyl group and C–C bond on benzene). For guest-free MMCF-4, the torsional degree range was 72° ($\Delta t_d = 72^\circ$), indicating existence of considerable vibration modes. However, once upon MA molecules attached, dramatic reduction of vibrations (distribution range of torsional degrees) was observed ($\Delta t_d = 35^\circ$), due to the strong bifurcate hydrogen bonding formation. This manifested apparently that the hydrogen bond interactions restrict the intrinsic vibrations, reducing nonradiative decay pathways and consequently achieving enhancement of emission. In another aspect, the replacement of interacted H_2O by MA was also considered here. According to previous studies and our experimental results, the OH oscillators on the second coordination sphere could still, although with very low efficiency, quench the lanthanide emission. However, unlike the replacement of coordinating H_2O in organic solvents to recover the emission intensity, the binding of methyl amine on H-bond interacting sites in aqueous environment should be regarded as an extension of the primary coordination sphere, which further blocks the H_2O molecules away from the emission center and thus results in a recovery of emission strength. Both scenarios are based on the inaccessible first coordination sphere as well as interacting sites-decorated second coordination sphere, which may come up simultaneously in the practical circumstance.

Electron transfer contributes in most cases for lanthanide fluorescence quenching and was proposed here as the main mechanism for the quenching behaviors in 6-MP@MMCF-4.^[8d-k, 20d, 21] Based on the results obtained from molecular orbital calculations, bottom of the LUMO energy states of H_6L lies above the LUMO energies of 6-MP, allowing efficient electron transfers from the antenna to analytes (Table S5). Thus, the quenching of MMCF-4 by 6-MP was confirmed to arise through photoinduced electron transfer (PET). More importantly, we found additional interactions

between 6-MP and the channel surface in MMCF-4, which are favorable to detect analytes in ultra-low concentration. Aiming at obtaining snapshots about the configurations of this highly efficient quenching, crystallographic studies were also performed for the structural visualization of 6-MP@MMCF-4. As shown in Figure 4, the adsorbed 6-MP molecules display a side-on adsorption mode within the channel of MMCF-4, being recognized by chelate oxygens and stabilized into the channels through N–H...O bonding together with hydrogen- π interactions. An in-depth analysis shows the acting site on 6-MP is the protonated N in pyrimidine ring, which forms bifurcated hydrogen-bond with chelate oxygen atoms with distances of 2.62 and 2.84 Å, respectively. Besides, the pyrimidine moiety from 6-MP interacts with the phenyl substituent of the ligand at a distance reasonable for hydrogen- π interaction (3.40 Å). The structure directing ability of the channels in MMCF-4 could redirect 6-MP adjacently, thus enabling high efficiency photoinduced electron transfer (PET) process. As existing in many molecular recognition events, these direct contacts between 6-MP and MMCF-4 have a profound effect of imposing preferential configurations and a high degree of loading for guests, which could interpret the sensitive detection of MMCF-4 toward 6-MP.

Conclusion

A second-sphere interaction mechanism has been proved to be highly effective to achieve turn-on sensing in Ln-MOFs. This work, to the best of our knowledge, is the first case in MOFs for turn-on sensing of organic analytes in aqueous environment through second-sphere modulation of lanthanide chromophores. The ligand design ensured well-shielded terbium node while efficient correspondence with binding sites densely populated on second-coordination sphere. The obtained MMCF-4 exhibited an ultralow detection limit of

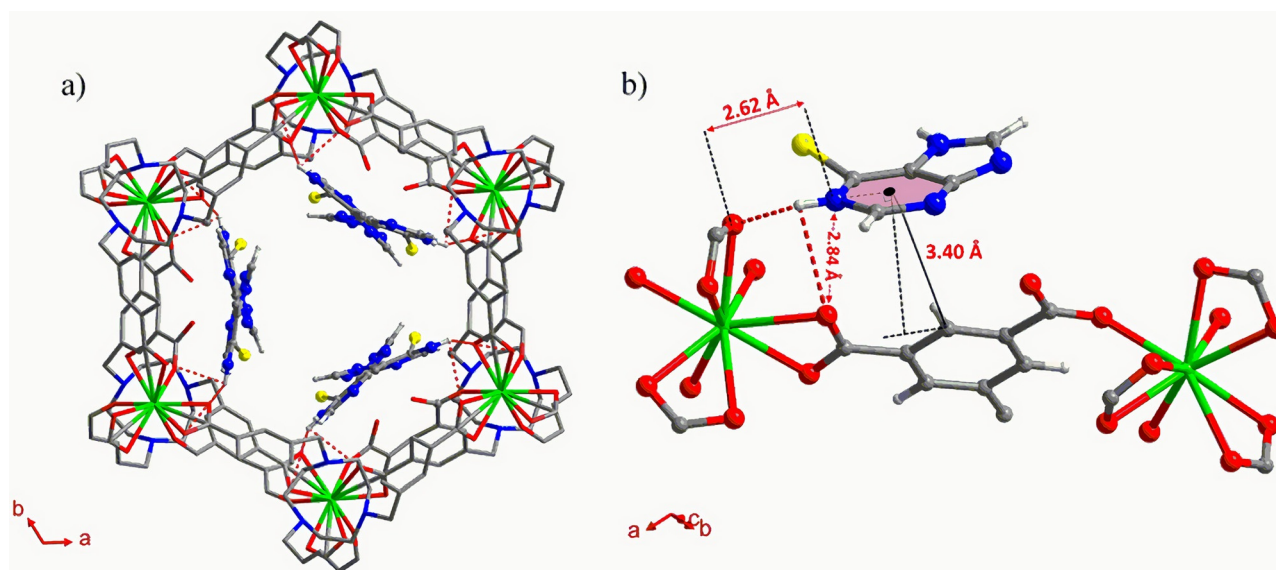


Figure 4. a) Perspective view of a single pore in 6-MP@MMCF-4 by SCXRD analysis, along the c axis, showing 6-MP guest molecules held in MMCF-4.^[22] b) Details of host-guest interactions in 6-MP@MMCF-4.

86 nM toward MA in aqueous solutions. Strong interactions formed when MA diffused into MMCF-4 and hydrogen bonded with L, and thus lead to ligand rigidification, which suppressed manifold nonradiative decay pathways. Such mechanism was confirmed by single-crystal X-ray diffraction analysis and molecular dynamic simulations. Besides, this second-sphere interactions could also be applied to turn-off detection, which excludes the interferences in aqueous circumstances, increases the local concentration of analyte and renders a sensitive detection of 6-MP. This investigation therefore opens new opportunities for lanthanide chromophores as an efficient fluorescence platform with novel sensing behaviors in a wide range of applications.

Acknowledgements

The authors acknowledge the Robert A. Welch Foundation (B-0027) for financial support of this work. The authors also extended their sincere appreciation to Researchers Supporting Program project no (RSP-2021/79) at King Saud University, Riyadh, Saudi Arabia for partially funding this work (A.N.).

Conflict of Interest

The authors declare no conflict of interest.

Keywords: lanthanides · metal–organic frameworks · second-sphere interaction · selective sensing · turn-on fluorescence

- [1] a) R. Joseph, C. P. Rao, *Chem. Rev.* **2011**, *111*, 4658–4702; b) J. Hu, S. Liu, *Acc. Chem. Res.* **2014**, *47*, 2084–2095; c) J. J. Lavigne, E. V. Anslyn, *Angew. Chem. Int. Ed.* **2001**, *40*, 3118–3130; *Angew. Chem.* **2001**, *113*, 3212–3225.
- [2] a) Y. Zhang, S. Yuan, G. Day, X. Wang, X. Yang, H.-C. Zhou, *Coord. Chem. Rev.* **2018**, *354*, 28–45; b) H. Wang, W. P. Lustig, J. Li, *Chem. Soc. Rev.* **2018**, *47*, 4729–4756; c) L. E. Kreno, K. Leong, O. K. Farha, M. Allendorf, R. P. Van Duyne, J. T. Hupp, *Chem. Rev.* **2012**, *112*, 1105–1125; d) N. B. Shustova, A. F. Cozzolino, S. Reineke, M. Baldo, M. Dinca, *J. Am. Chem. Soc.* **2013**, *135*, 13326–13329.
- [3] A. Okrut, R. C. Runnebaum, X. Ouyang, J. Lu, C. Aydin, S. J. Hwang, S. Zhang, O. A. Olatunji-Ojo, K. A. Durkin, D. A. Dixon, B. C. Gates, A. Katz, *Nat. Nanotechnol.* **2014**, *9*, 459–465.
- [4] R. Kostecki, S. Heng, A. M. Mak, H. Ebendorff-Heidepriem, T. M. Monro, A. D. Abell, *ACS Appl. Mater. Interfaces* **2018**, *10*, 41866–41870.
- [5] Y. Li, S. Zhang, D. Song, *Angew. Chem. Int. Ed.* **2013**, *52*, 710–713; *Angew. Chem.* **2013**, *125*, 738–741.
- [6] D. Wu, Z. Zhang, X. Chen, L. Meng, C. Li, G. Li, X. Chen, Z. Shi, S. Feng, *Chem. Commun.* **2019**, *55*, 14918–14921.
- [7] T. Y. Luo, P. Das, D. L. White, C. Liu, A. Star, N. L. Rosi, *J. Am. Chem. Soc.* **2020**, *142*, 2897–2904.
- [8] a) H. Furukawa, K. E. Cordova, M. O’Keeffe, O. M. Yaghi, *Science* **2013**, *341*, 1230444; b) C. Valente, E. Choi, M. E. Belowich, C. J. Doonan, Q. Li, T. B. Gasa, Y. Y. Botros, O. M. Yaghi, J. F. Stoddart, *Chem. Commun.* **2010**, *46*, 4911–4913; c) B. Chen, S. Xiang, G. Qian, *Acc. Chem. Res.* **2010**, *43*, 1115–1124; d) J. Rocha, L. D. Carlos, F. A. Paz, D. Ananias, *Chem. Soc. Rev.* **2011**, *40*, 926–940; e) Y. Cui, Y. Yue, G. Qian, B. Chen, *Chem. Rev.* **2012**, *112*, 1126–1162; f) Z. Hu, B. J. Deibert, J. Li, *Chem. Soc. Rev.* **2014**, *43*, 5815–5840; g) Y. Cui, B. Chen, G. Qian, *Coord. Chem. Rev.* **2014**, *273*–274, 76–86; h) B. Yan, *Acc. Chem. Res.* **2017**, *50*, 2789–2798; i) A. D. G. Firmino, F. Figueira, J. P. C. Tomé, F. A. A. Paz, J. Rocha, *Coord. Chem. Rev.* **2018**, *355*, 133–149; j) E. A. Dolgoplova, A. M. Rice, C. R. Martin, N. B. Shustova, *Chem. Soc. Rev.* **2018**, *47*, 4710–4728; k) S. Wu, H. Min, W. Shi, P. Cheng, *Adv. Mater.* **2020**, *32*, 1805871; l) A. Mallick, A. M. El-Zohry, O. Shekhah, J. Yin, J. Jia, H. Aggarwal, A. H. Emwas, O. F. Mohammed, M. Eddaoudi, *J. Am. Chem. Soc.* **2019**, *141*, 7245–7249; m) C. Y. Liu, X. R. Chen, H. X. Chen, Z. Niu, H. Hirao, P. Braunstein, J. P. Lang, *J. Am. Chem. Soc.* **2020**, *142*, 6690–6697.
- [9] a) Y. Cui, R. Song, J. Yu, M. Liu, Z. Wang, C. Wu, Y. Yang, Z. Wang, B. Chen, G. Qian, *Adv. Mater.* **2015**, *27*, 1420–1425; b) B. Chen, L. Wang, F. Zapata, G. Qian, E. B. Lobkovsky, *J. Am. Chem. Soc.* **2008**, *130*, 6718–6719; c) Y. Cui, H. Xu, Y. Yue, Z. Guo, J. Yu, Z. Chen, J. Gao, Y. Yang, G. Qian, B. Chen, *J. Am. Chem. Soc.* **2012**, *134*, 3979–3982; d) B. V. Harbuzaru, A. Corma, F. Rey, J. L. Jorda, D. Ananias, L. D. Carlos, J. Rocha, *Angew. Chem. Int. Ed.* **2009**, *48*, 6476–6479; *Angew. Chem.* **2009**, *121*, 6598–6601; e) S. Y. Zhang, W. Shi, P. Cheng, M. J. Zaworotko, *J. Am. Chem. Soc.* **2015**, *137*, 12203–12206; f) H. Xu, C. S. Cao, X. M. Kang, B. Zhao, *Dalton Trans.* **2016**, *45*, 18003–18017.
- [10] H. Q. Yin, X. Y. Wang, X. B. Yin, *J. Am. Chem. Soc.* **2019**, *141*, 15166–15173.
- [11] a) D. Parker, P. K. Senanayake, J. A. G. Williams, *J. Chem. Soc. Perkin Trans. 2* **1998**, 2129–2139; b) M. L. Cable, J. P. Kirby, K. Sorasaene, H. B. Gray, A. Ponce, *J. Am. Chem. Soc.* **2007**, *129*, 1474–1475.
- [12] a) D. Parker, *Coord. Chem. Rev.* **2000**, *205*, 109–130; b) D. Parker, R. S. Dickins, H. Puschmann, C. Crossland, J. A. K. Howard, *Chem. Rev.* **2002**, *102*, 1977–2010.
- [13] a) A. de Bettencourt-Dias, R. M. Beeler, J. R. Zimmerman, *Inorg. Chem.* **2020**, *59*, 151–160; b) I. Ling, C. L. Raston, *Coord. Chem. Rev.* **2018**, *375*, 80–105.
- [14] B. P. Murphy, L. Quinti, D. G. Kelly, W. J. Martin, A. Perotti, M. B. Hursthouse, T. Gelbrich, *Inorg. Chem. Commun.* **2002**, *5*, 577–580.
- [15] a) L. G. Nielsen, A. K. R. Junker, T. J. Sorensen, *Dalton Trans.* **2018**, *47*, 10360–10376; b) S. Aimea, A. Bargea, M. Bottaa, M. Fasanoa, J. D. Ayalab, G. Bombieribq, *Inorg. Chim. Acta* **1996**, *246*, 423–429; c) A. Beeby, I. M. Clarkson, R. S. Dickins, S. Faulkner, D. Parker, L. Royle, A. S. de Sousa, J. A. G. Williams, M. Woods, *J. Chem. Soc. Perkin Trans. 2* **1999**, 493–503; d) S. Bhattacharya, S. Bala, R. Mondal, *CrystEngComm* **2019**, *21*, 5665–5672.
- [16] a) G. K. Ramachandran, W. P. Yong, C. H. Yeow, *PLoS One* **2016**, *11*, 0162222; b) T. Gao, E. S. Tillman, N. S. Lewis, *Chem. Mater.* **2005**, *17*, 2904–2911; c) Y. Yi, X. Zhou, L. Xue, W. Wang, *Environ. Chem. Lett.* **2018**, *16*, 1083–1088; d) S. S. Lv, S. K. Miao, Y. Ma, M. M. Zhang, Y. Wen, C. Y. Wang, Y. P. Zhu, W. Huang, *J. Phys. Chem. A* **2015**, *119*, 8657–8666; e) S. H. Zeisel, K. A. DaCosta, *Cancer Res.* **1986**, *46*, 6136–6138.
- [17] M. Ding, X. Cai, H. L. Jiang, *Chem. Sci.* **2019**, *10*, 10209–10230.
- [18] L. Lennard, *Eur. J. Clin. Pharmacol.* **1992**, *43*, 329–339.
- [19] H. Kanemitsu, H. Yamauchi, M. Komatsu, S. Yamamoto, S. Okazaki, K. Uchida, H. Nakayama, *Neurotoxicol. Teratol.* **2009**, *31*, 104–109.
- [20] a) R. B. Lin, Y. He, P. Li, H. Wang, W. Zhou, B. Chen, *Chem. Soc. Rev.* **2019**, *48*, 1362–1389; b) T. Steiner, *Angew. Chem. Int. Ed.* **2002**, *41*, 48–76; *Angew. Chem.* **2002**, *114*, 50–80; c) S. Wu, Y. Lin, J. Liu, W. Shi, G. Yang, P. Cheng, *Adv. Funct. Mater.* **2018**, *28*, 1707169; d) B. Wang, P. Wang, L. H. Xie, R. B. Lin, J. Lv, J. R. Li, B. Chen, *Nat. Commun.* **2019**, *10*, 3861.

[21] Z. Hu, W. P. Lustig, J. Zhang, C. Zheng, H. Wang, S. J. Teat, Q. Gong, N. D. Rudd, J. Li, *J. Am. Chem. Soc.* **2015**, *137*, 16209–16215.

[22] Deposition Numbers 2052009 (for MMCF-4), 2025814 (for MA@MMCF-4), and 2025815 (for 6-MP@MMCF-4) contain the supplementary crystallographic data for this paper. These data are provided free of charge by the joint Cambridge Crystallographic Data Centre and Fachinformationszentrum

Karlsruhe Access Structures service www.ccdc.cam.ac.uk/structures.

Manuscript received: June 3, 2021

Revised manuscript received: July 20, 2021

Accepted manuscript online: August 24, 2021

Version of record online: September 20, 2021